

LARGE-SCALE POWER SPECTRUM FROM PECULIAR VELOCITIES VIA LIKELIHOOD ANALYSIS

Saleem Zaroubi¹, Idit Zehavi², Avishai Dekel^{1,2},
Yehuda Hoffman² & Tsafrir Kolatt^{3,4}

¹Astronomy Department and Center for Particle Astrophysics, University of California, Berkeley, CA 94720

²Racah Institute of Physics, The Hebrew University, Jerusalem 91904, Israel

³Harvard-Smithsonian Center for Astrophysics, 60 Garden St., Cambridge MA 02138

⁴UCO/Lick Observatory, University of California, Santa Cruz, CA 95064

ABSTRACT

The power spectrum (PS) of *mass* density fluctuations, independent of “biasing”, is estimated from the Mark III catalog of peculiar velocities using Bayesian statistics. A parametric model is assumed for the PS, and the free parameters are determined by maximizing the probability of the model given the data. The method has been tested using detailed mock catalogs. It has been applied to generalized CDM models with and without COBE normalization.

The robust result for all the models is a relatively high PS, with $P(k)\Omega^{1.2} = (4.8 \pm 1.5) \times 10^3 (h^{-1}\text{Mpc})^3$ at $k = 0.1 h \text{Mpc}^{-1}$. An extrapolation to smaller scales using the different CDM models yields $\sigma_8\Omega^{0.6} = 0.88 \pm 0.15$. The peak is weakly constrained to the range $0.02 \leq k \leq 0.06 h \text{Mpc}^{-1}$. These results are consistent with a direct computation of the PS (Kolatt & Dekel 1996). When compared to galaxy-density surveys, the implied values for β ($\equiv \Omega^{0.6}/b$) are of order unity to within 25%.

The parameters of the COBE-normalized, flat CDM model are confined by a 90% likelihood contour of the sort $\Omega h_{50}^\mu n^\nu = 0.8 \pm 0.2$, where $\mu = 1.3$ and $\nu = 3.4, 2.0$ for models with and without tensor fluctuations respectively. For open CDM the powers are $\mu = 0.95$ and $\nu = 1.4$ (no tensor fluctuations). A Γ -shape model free of COBE normalization yields only a weak constraint: $\Gamma = 0.4 \pm 0.2$.

Subject headings: cosmology: theory — cosmology: observation — dark matter — galaxies: clustering — galaxies: distances and redshifts — large scale structure of universe

1. INTRODUCTION

In the standard picture of cosmology, the structure on large scales originated from small-amplitude initial density fluctuations that were amplified by gravitational instability. These initial fluctuations are assumed to be a Gaussian random field, solely characterized by its power spectrum. On large scales, the fluctuations are linear even at late times, so that the power spectrum preserves its original shape. This makes it a very useful statistics for large-scale structure.

The power spectra of galaxy density were derived for many different samples, in two angular dimensions or in three dimensions from redshift space. Unfortunately, these power spectra correspond to objects that are not necessarily unbiased tracers of the underlying mass distribution, and it is the mass distribution that is directly related to theory (*e.g.* Dekel & Rees 1987 for a review on “galaxy biasing”). Clear evidence for this bias is provided by the fact that galaxies of different types are observed to cluster differently (*e.g.* Dressler 1980). It would therefore be naive to assume that any of the galaxy power spectra directly reflects the mass PS. Furthermore, in estimates of the galaxy PS from redshift surveys, uncertainties also arise when correcting for redshift distortions (Kaiser 1987, Zaroubi and Hoffman 1996). For these reasons, one wishes to measure the mass PS directly from dynamical data, bypassing the complex galaxy-biasing issues and the need to correct for redshift distortions. In principle, such dynamical information can be provided by peculiar velocities, by gravitational lensing effects, or by fluctuations in the cosmic microwave background (CMB). In particular, the accumulating catalogs of galaxy peculiar velocities enable a direct determination of the mass PS under the natural assumption that the galaxies are unbiased tracers of the large-scale, gravitationally-induced velocity field.

The PS is computed here from the Mark III catalog of peculiar velocities (Willick *et al.* 1995 WI; 1996a WII; 1996b WIII), which consists of more than 3000 galaxies. It was compiled from several different data sets of spiral and elliptical/S0 galaxies with distances inferred by the forward Tully-Fisher and $D_n-\sigma$ methods. These data were re-calibrated and self-consistently put together as a homogeneous catalog for velocity analysis. The catalog provides radial peculiar velocities and inferred distances with errors on the order of 17–21% of the distance per galaxy, sampled nonuniformly out to distances of $\sim 80 h^{-1}\text{Mpc}$ from the Local Group.

The catalog exists in two versions that differ by the method of correction for Malmquist bias. In the standard “G” version, the galaxies are first heavily grouped into ~ 1200 objects ranging from isolated field galaxies to rich clusters. The grouping reduces the non-linear noise on small scales and the resulting Malmquist bias. Then the data are systematically corrected for the Malmquist bias (see Dekel 1994). As a reference, we also use the “S” version, where a more straightforward systematic correction is applied to the field galaxies as singles, at the expense of larger noise on small scales.

These data allow a reasonable recovery of the dynamical fields with $\sim 12 h^{-1}\text{Mpc}$ smoothing in a sphere of radius $\sim 60 h^{-1}\text{Mpc}$ about the Local Group, extending to $\sim 80 h^{-1}\text{Mpc}$ in certain regions. The POTENT method (Bertschinger & Dekel 1989; Dekel, Bertschinger & Faber 1990; Dekel 1994, 1997) attempts a recovery of the underlying density field with fixed Gaussian smoothing within this volume. In an associated paper, Kolatt and

Dekel (1996, KD) have computed the mass PS from the smoothed density field recovered by POTENT from Mark III. The limitations of the data introduce severe systematic errors, that were modeled via Monte-Carlo mock catalogs and then used to correct the measured PS. Since the KD results naturally involve uncertainties, an independent estimate of the PS, using a very different method, is useful.

Our purpose is to estimate the mass PS directly from the peculiar velocities of the Mark III catalog, by means of a likelihood analysis. The non-local nature of the peculiar velocities, *i.e.* being influenced by the mass distribution in a whole neighborhood, allows one to probe scales somewhat larger than those probed by the density field. For example, the effect of a bulk velocity across the entire volume is not evident if only the density field is considered. For a similar reason, the velocity field is expected to obey linear theory better than the density field smoothed on a comparable scale, and to closer resemble a Gaussian field. Our approach here does not involve any explicit window function, weighting or smoothing, nor does it require artificial binning of the PS. In addition, it automatically underweights noisy, unreliable data.

The data analyzed here are especially suited for Bayesian analysis. The sparse and inhomogeneous sampling of a random Gaussian field with Gaussian errors yields a multivariate Gaussian data set. The corresponding *posterior* probability distribution function (PDF) is a multivariate Gaussian that is completely determined by the assumed PS and the assumed covariance matrix of errors. Under these conditions one can write the joint PDF of the model PS and the underlying velocity or density field, and then simultaneously estimate the PS model parameters and recover the “Wiener filter” solution of the fields (Zaroubi *et al.* 1995). In an associated paper (Zaroubi, Hoffman & Dekel 1996), we present the high-resolution fields recovered from this same data set using the PS derived here.

To apply our method, the simplifying assumptions that have to be made are (a) that the peculiar velocities are drawn from a Gaussian field, (b) that their correlation function can be derived from the density PS using linear theory, and (c) that the errors are Gaussian and accurately estimated. The need to assume a parametric functional form for the PS is also a limitation; one can try to achieve flexibility by using a large number of parameters and a variety of functional forms, but at the risk of making the likelihood analysis unstable in some cases (§5).

The method is described in §2, where the relation between the PS and the velocity correlation functions is specified, and the likelihood algorithm for computing the PS is described. The method is tested using a mock catalog in §3. The resultant power spectra are presented in §4, as derived from the Mark III data alone, and for generalized CDM models imposing COBE normalization. The associated constraints on the cosmological parameters are analyzed. Our conclusions are summarized and discussed in §5.

2. METHOD

2.1. Velocity Correlations

The computation of the matter power spectrum from the peculiar velocity data by means of likelihood analysis requires a relation between the velocity correlation function and the power spectrum. Define the two-point velocity correlation (3×3) tensor by the

average over all pairs of points \mathbf{r}_i and \mathbf{r}_j that are separated by $\mathbf{r} = \mathbf{r}_j - \mathbf{r}_i$,

$$\Psi_{\mu\nu}(\mathbf{r}) \equiv \langle v_\mu(\mathbf{r}_i) v_\nu(\mathbf{r}_j) \rangle, \quad (1)$$

where $v_\mu(\mathbf{r}_i)$ is the μ component of the peculiar velocity at \mathbf{r}_i . In linear theory, it can be expressed in terms of two scalar functions of $r = |\mathbf{r}|$ (Górski 1988), parallel and perpendicular to the separation \mathbf{r} ,

$$\Psi_{\mu\nu}(\mathbf{r}) = \Psi_\perp(r) \delta_{\mu\nu} + [\Psi_\parallel(r) - \Psi_\perp(r)] \hat{\mathbf{r}}_\mu \hat{\mathbf{r}}_\nu. \quad (2)$$

The spectral representation of these radial correlation functions is

$$\Psi_{\perp,\parallel}(r) = \frac{H_0^2 f^2(\Omega)}{2\pi^2} \int_0^\infty P(k) K_{\perp,\parallel}(kr) dk, \quad (3)$$

where $K_\perp(x) = j_1(x)/x$ and $K_\parallel(x) = j_0 - 2j_1(x)/x$, with $j_l(x)$ the spherical Bessel function of order l . The cosmological Ω dependence enters as usual in linear theory via $f(\Omega) \approx \Omega^{0.6}$, and H_0 is the Hubble constant. A parametric functional form of $P(k)$ thus translates to a parametric form of $\Psi_{\mu\nu}$.

2.2. Likelihood Analysis

Let \mathbf{m} be the vector of model parameters and \mathbf{d} the vector of N data points. Then Bayes theorem states that the *posterior* probability density of a model given the data is

$$\mathcal{P}(\mathbf{m}|\mathbf{d}) = \frac{\mathcal{P}(\mathbf{m})\mathcal{P}(\mathbf{d}|\mathbf{m})}{\mathcal{P}(\mathbf{d})}. \quad (4)$$

The denominator is merely a normalization constant. The probability density of the model parameters, $\mathcal{P}(\mathbf{m})$, is unknown, and in the absence of any other information we assume it is uniform within a certain range. The conditional probability of the data given the model, $\mathcal{P}(\mathbf{d}|\mathbf{m})$, is the likelihood function, $\mathcal{L}(\mathbf{d}|\mathbf{m})$. The objective in this approach, which is finding the set of parameters that maximizes the probability of the model given the data, is thus equivalent to maximizing the likelihood of the data given the model (Kaiser 1988; see also Jaffe & Kaiser 1994 for a first application to the Lauer & Postman data).

The Bayesian analysis measures the relative likelihood of different models. An absolute frequentist measure of goodness of fit could be provided by the Chi-square per degree of freedom, which we use as a check on the best parameters obtained by the likelihood analysis.

Assuming that the velocities form a Gaussian random field, the two-point velocity correlation tensor Ψ fully characterizes the statistics of the velocity field. Define the radial-velocity correlation ($N \times N$) matrix U_{ij} by $U_{ij} = \hat{\mathbf{r}}_i^\dagger \Psi \hat{\mathbf{r}}_j$, where i and j refer to the data points. Let the inferred radial peculiar velocity at \mathbf{r}_i be u_i , with the corresponding error ϵ_i also assumed to be a Gaussian random variable. The observed correlation matrix is then $\tilde{U}_{ij} = U_{ij} + \epsilon_i^2 \delta_{ij}$, and the likelihood of the N data points is

$$\mathcal{L} = [(2\pi)^N \det(\tilde{U}_{ij})]^{-1/2} \exp \left(-\frac{1}{2} \sum_{i,j}^N u_i \tilde{U}_{ij}^{-1} u_j \right). \quad (5)$$

Given that the correlation matrix, \tilde{U}_{ij} , is symmetric and positive definite, we can use the Cholesky decomposition method (*e.g.* Press *et al.* 1992) for computing the likelihood function (Eq. 5). The significant contribution of the errors to the diagonal terms makes the matrix especially well suited for decomposition. The calculation for a given choice of parameters and $N \sim 1200$ data points takes a few minutes on a Dec-Alpha workstation (of SpecFP92 ~ 150).

The likelihood function of Equation 5 is the posterior PDF of the parameters \mathbf{m} . It is a χ^2 distribution (with N degrees of freedom) with respect to the N data points, but it is not necessarily a χ^2 distribution with respect to the parameters. Therefore, the task of assigning accurate confidence levels to the parameters requires elaborate integrations over the volume encompassed by the equal-likelihood surfaces in parameter space. In the present paper we limit ourselves to a rough estimate of confidence levels by crudely approximating $-2\ln \mathcal{L}$ as a χ^2 distribution in parameter space.

An important feature of this method, which distinguishes it from other methods (*e.g.* KD), is that the formal likelihood errors include both the distance measurement errors and the cosmic scatter due to the finite discrete sampling.

Note that the grouping in the Mark III catalog also serves as a mean of smoothing over nonlinear velocities. The PS on large-scales should not be much affected by this grouping because when group galaxies enter the likelihood analysis as individuals, they enter with low weights compared to the weight of a whole group. For un-grouped galaxies, the noise term $\epsilon_i^2 \delta_{ij}$ is larger (relative to the signal U_{ij}) in the observed correlation matrix \tilde{U}_{ij} of Equation 5.

Note also that the quantity that can be derived from peculiar velocity data via the linear approximation is $f^2(\Omega) P(k)$, where $P(k)$ is the mass density PS (see Eq. 3).

3. TESTING THE METHOD

Careful testing of the method with realistic mock catalogs is essential in view of the large distance errors, the sparse and non-uniform sampling, the bias-correction procedures, and the possible non-linear and non-Gaussian effects.

The mock Mark III catalogs are described in Kolatt *et al.* (1996). They are based on simulations whose initial conditions were extracted from a reconstruction of the smoothed real-space density field from the IRAS 1.2Jy redshift survey, taken back into the linear regime. Small-scale perturbations were added by means of constrained random realizations. The system was then evolved forward in time using an N-body simulation assuming $\Omega = 1$, and stopped at two alternative times, when the *rms* density fluctuation in a top-hat sphere of radius $8 h^{-1} \text{Mpc}$ reached $\sigma_8 = 0.7$ and later when $\sigma_8 = 1.12$.

The “galaxies” in the simulation were identified via a linear biasing scheme ($b=1.35$), and they were divided into ‘spirals’ and ‘ellipticals’ according to Dressler’s morphology-density relation. The galaxies were assigned TF quantities (internal velocities and absolute magnitudes) that were Gaussianly scattered about an assumed TF relation, and were then “observed” following the selection criteria of the actual data sets that compose the Mark III catalog. The mock catalogs were grouped and corrected for biases just like the real

data, producing analogous G and S mock catalogs.

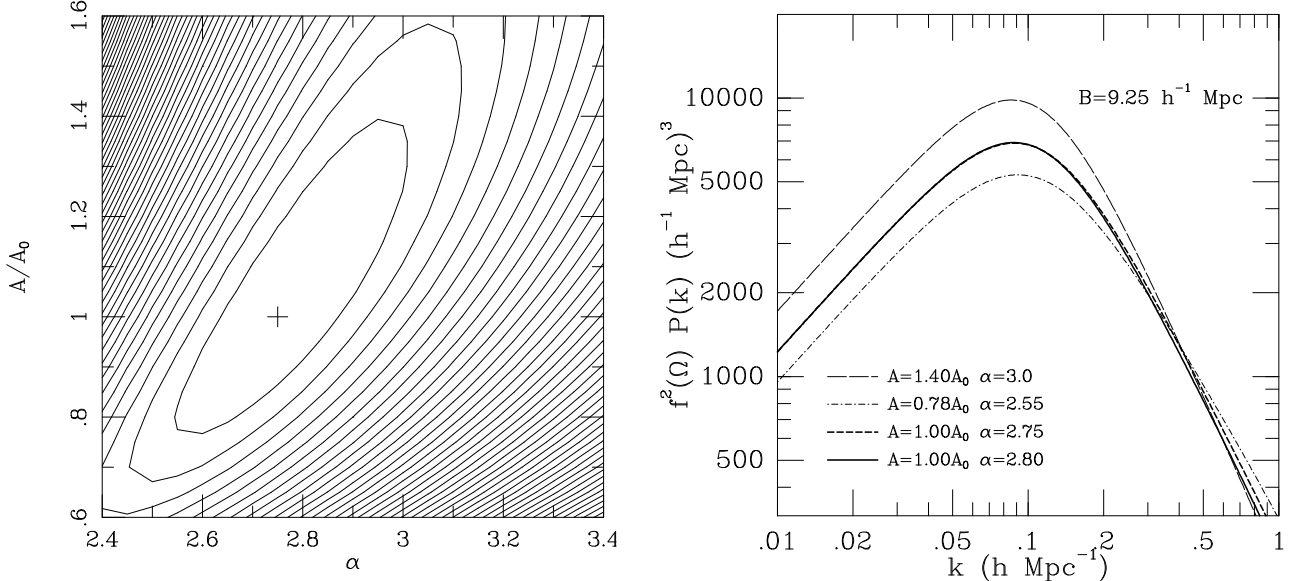


Figure 1a: Contour map of $\ln\mathcal{L}$ in the $\alpha - A$ plane for a mock catalog based on the parametric model of Equation 6 with $B=9.25 h^{-1} \text{Mpc}$. Contour spacing is $\Delta[\ln\mathcal{L}]=-1$. The best-fit point is marked.

Figure 1b: The true power spectrum of the simulation (heavy solid), compared with the best-fit solution (heavy dashed), and two power spectra whose parameters lie on the innermost closed contour of Figure 1a.

The true PS of the mass in the simulation is well approximated by the functional form

$$P(k) = \frac{A_0 k}{1 + (B k)^\alpha}, \quad (6)$$

with $A_0 = 4.68$ and $12.28 \times 10^4 (h^{-1} \text{Mpc})^4$, $B = 8.3$ and $9.25 h^{-1} \text{Mpc}$, and $\alpha = 3.2$ and 2.8 , for the $\sigma_8 = 0.7$ and 1.12 cases respectively.

The likelihood analysis was applied to the mock catalogs using the parametric functional form of Equation 6 as a prior. Only two parameters were allowed to vary at a time while the third parameter was kept fixed. Figure 1a shows, for example, a contour map of $\ln\mathcal{L}$ (relative to the maximum-likelihood peak) for one of the $\sigma_8 = 1.12$, G mock catalogs, spanning the $\alpha - A$ plane with $B = 9.25 h^{-1} \text{Mpc}$. The contours are separated by $\Delta[\ln\mathcal{L}] = -1$. Maximum likelihood is obtained at $A = A_0$ and $\alpha = 2.75$ (compared to 2.80). Assuming a χ^2 distribution with two degrees of freedom, the 90% confidence limit of the likelihood around the best-fit parameters is at $\ln\mathcal{L} \approx -2.3$. We conclude that the recovery method works well.

Figure 1b shows the recovered PS in comparison with the true PS of the simulation. They almost coincide over the whole range of scales, showing slight deviations only on very small scales. To illustrate the level of uncertainty, we plot for comparison two other power spectra that were obtained with parameter pairs that lie on the innermost contour about the maximum in Figure 1a. It shows that the amplitude near the peak can be off

by about 25%, and that the recovery becomes more robust at moderately smaller scales. The success of the recovery is similar when the other pairs of parameters are allowed to vary, and also when allowing all three parameters to vary at the same time.

Similar success was achieved when the method was applied to the S mock catalogs. In what follows we focus on the results from the G Mark III catalog, and refer to the S catalog as an indication for robustness.

4. RESULTS

4.1. The Γ Model

We first recover the PS from the velocity data alone, independent of COBE normalization. We use as a parametric prior the so-called Γ model (*e.g.* Efstathiou, Bond and White 1992),

$$P(k) = A k T^2(k), \quad T(k) = \left(1 + [ak/\Gamma + (bk/\Gamma)^{3/2} + (ck/\Gamma)^2]^\nu\right)^{-1/\nu}, \quad (7)$$

with $a = 6.4 h^{-1}\text{Mpc}$, $b = 3.0 h^{-1}\text{Mpc}$, $c = 1.7 h^{-1}\text{Mpc}$ and $\nu = 1.13$. The free parameters to be determined by the likelihood analysis are the normalization factor A and the Γ parameter. In the context of the CDM cosmological model, Γ has a specific cosmological interpretation, $\Gamma = \Omega h$. Here, however, independently of CDM, Equation 7 serves as a generic function with logarithmic slopes $n = 1$ and -3 on large and small scales respectively, and with a turnover at some intermediate wavenumber that is determined by the single shape parameter Γ .

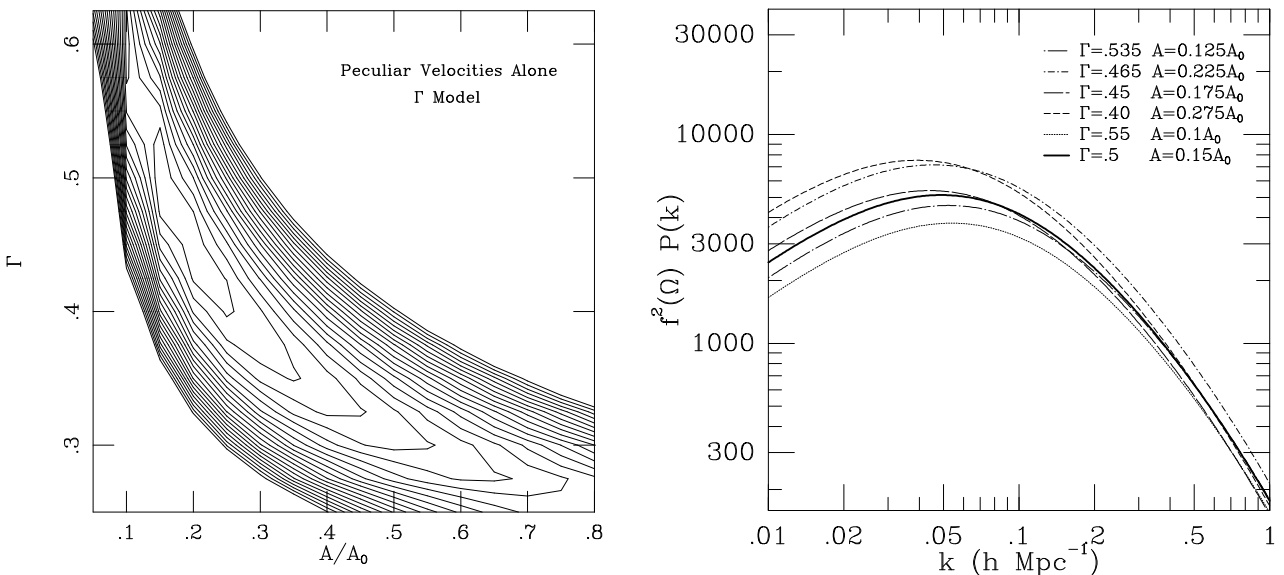


Figure 2a: Contour map of $\ln \mathcal{L}$ for the Γ model. Contour spacing is $\Delta[\ln \mathcal{L}] = -1$. A in units of $A_0 = 2.0 \times 10^6 (h^{-1}\text{Mpc})^4$.

Figure 2b: The most likely Γ -model power spectrum (solid), and five other models whose parameters lie on the innermost contour of Figure 2a.

Figure 2a shows the contour map of $\ln \mathcal{L}$ in the $A - \Gamma$ plane. The maximum likelihood values are $\Gamma = 0.5 \pm 0.15$ and $A = 3.0 \times 10^5 (h^{-1} \text{Mpc})^4$. The corresponding value of $\sigma_8 \Omega^{0.6}$ is 0.85 ± 0.1 . The error-bars quoted here (and throughout the paper) are the 90% confidence limits. Figure 2b shows the best-fit PS (solid). To illustrate the uncertainty in the PS we also show the power spectra of five other parameter pairs that lie on the innermost likelihood contour about the best fit (roughly the 65% confidence limit). We find the estimate of $\sigma_8 \Omega^{0.6}$ to be robust to the grouping of the data. On the other hand, the estimate of Γ without imposing COBE normalization is sensitive to the grouping; for the S catalog we obtain $\Gamma = 0.3 \pm 0.1$.

4.2. COBE-Normalized CDM Models

We now restrict our attention to the generalized family of CDM cosmological models, allowing variations in the cosmological parameters Ω , Λ and h , as well as the large-scale PS slope n and the contribution of tensor fluctuations. Furthermore, we now impose the normalization implied by the four-year COBE DMR data (Hinshaw *et al.* 1996) as an additional external constraint. The general form of the PS in these models is

$$P(k) = A_{COBE}(n, \Omega, \Lambda) T^2(\Omega, \Omega_B, h; k) k^n, \quad (8)$$

where we adopt the CDM transfer function proposed by Sugiyama (1995, a slight modification of Bardeen *et al.* 1986):

$$T(k) = \frac{\ln(1 + 2.34q))}{2.34q} \left[1 + 3.89q + (16.1q)^2 + (5.46q)^3 + (6.71q)^4 \right]^{-1/4}, \quad (9a)$$

$$q = k \left[\Omega h \exp(-\Omega_b - h_{50}^{1/2} \Omega_b / \Omega) (h \text{ Mpc}^{-1}) \right]^{-1} \quad (9b)$$

($h_{50} \equiv H_0/50 \text{ km s}^{-1} \text{Mpc}^{-1} = 2h$). The parameters are varied, two at a time, such that they span the range of currently popular CDM models, including Tilted- Λ CDM (flat: $\Omega + \Lambda = 1$, $\Omega \leq 1$, $n \leq 1$) and Tilted-Open CDM ($\Lambda = 0$, $\Omega \leq 1$, $n \leq 1$). We allow the possibility of nonzero tensor fluctuations, $T/S = 7(1 - n)$, where the ratio is of quadrupole moments (C_2) of tensor and scalar modes in the expansion of angular temperature fluctuations. (e.g. Turner 1993; Crittenden *et al.* 1993). In all cases, the baryonic density is assumed to be $\Omega_b = 0.024h^{-2}$ (e.g. Tytler *et al.* 1996).

The COBE normalization for each model has been calculated by various authors (Górski *et al.* 1995; Sugiyama 1995; White & Bunn 1995), using different Boltzmann codes, different statistical analyses, and sometimes even different temperature maps. We have arbitrarily adopted Sugiyama's normalization as a backbone, and for models not studied by him we use the other results after matching them to Sugiyama's, using the models that they have investigated in common.

In particular, the COBE normalization is modeled by $A_{COBE} = A_1(\Omega) A_2(n)$. For Tilted- Λ CDM models we use the fits:

$$\begin{aligned} \log A_1(\Omega) = & 7.83 - 8.33\Omega + 21.31\Omega^2 - 29.67\Omega^3 + 10.65\Omega^4 + 15.42\Omega^5 - \\ & 6.04\Omega^6 - 13.97\Omega^7 + 8.61\Omega^8, \end{aligned} \quad (10a)$$

$$\log A_2(n) = \begin{cases} -2.78 + 2.78n & T/S = 0 \\ -4.54 + 4.54n & T/S \neq 0 \end{cases} . \quad (10b)$$

These fits are for $h = 0.5$, but the h dependence in the range of interest is weak, and we ignore it here. For Tilted-Open CDM model with $T/S = 0$ the fit is:

$$\log A_1(\Omega) = 5.70 + 1.68\Omega - 4.53\Omega^2 + 7.57\Omega^3 - 7.53\Omega^4 + 3.15\Omega^5 - 0.23\Omega^6, \quad (11a)$$

$$\log A_2(n) = -2.71 + 2.71n. \quad (11b)$$

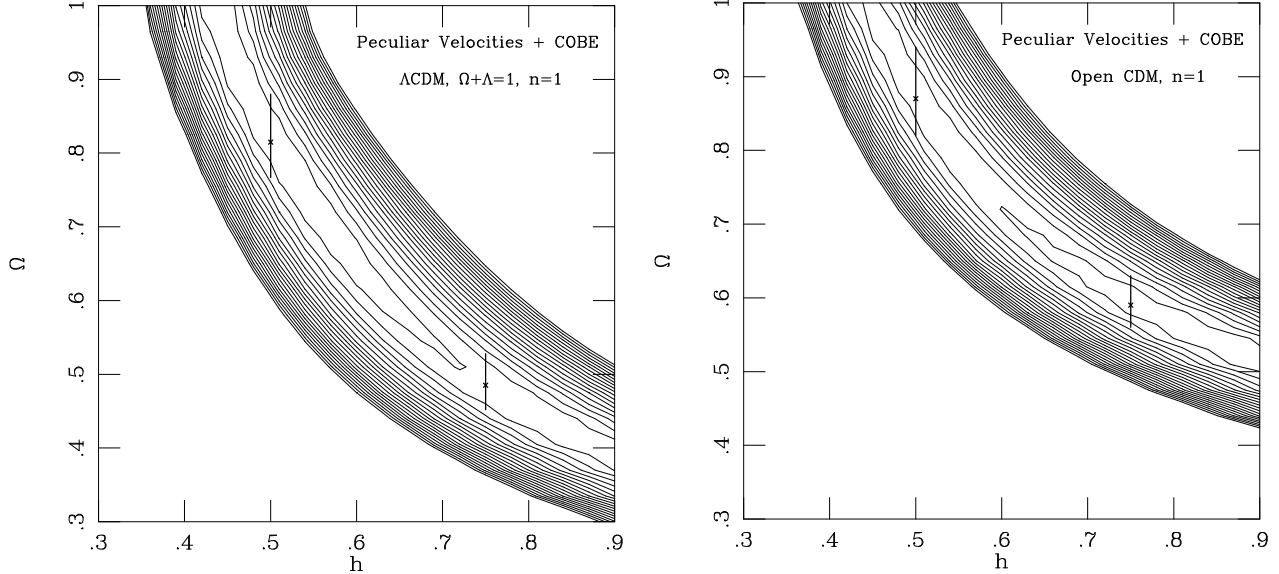


Figure 3: Contour map of \ln -likelihood in the $h - \Omega$ plane for the Λ CDM (a) and OCDM (b) models with $n=1$. $\Delta[\ln \mathcal{L}] = -1$. Shown are the most likely values of Ω for two fixed values of h , and the error bars corresponding to 90% confidence level.

4.2.1 Scale-Invariant Models

Figure 3 shows the likelihood contour map, in the $h - \Omega$ plane, for the flat CDM (Λ CDM) and Open CDM (OCDM) families of models with $n = 1$ (four-year COBE normalization by Sugiyama). It is clear from the elongated contour pattern that Ω and h are not constrained very effectively independently of each other. It is a degenerate combination of the two parameters that is being tightly determined by the elongated ridge of high likelihood. The constraints in the range plotted can be approximated (eye-ball fit) by the functional form

$$\Omega h_{50}^{1.3} = 0.83 \pm 0.09, \quad \Lambda CDM, \quad (12a)$$

$$\Omega h_{50}^{0.95} = 0.88 \pm 0.07, \quad OCDM. \quad (12b)$$

Also marked in Figure 3 are the most likely values of Ω for fixed given values of $h = 0.5$ and $h = 0.75$, and the corresponding one-dimensional error bars. The apparent weak preferences for high Ω (Λ CDM) or high h (OCDM) along the ridges of high likelihood is insignificant. In fact, it is not robust to changes between the G and S catalogs.

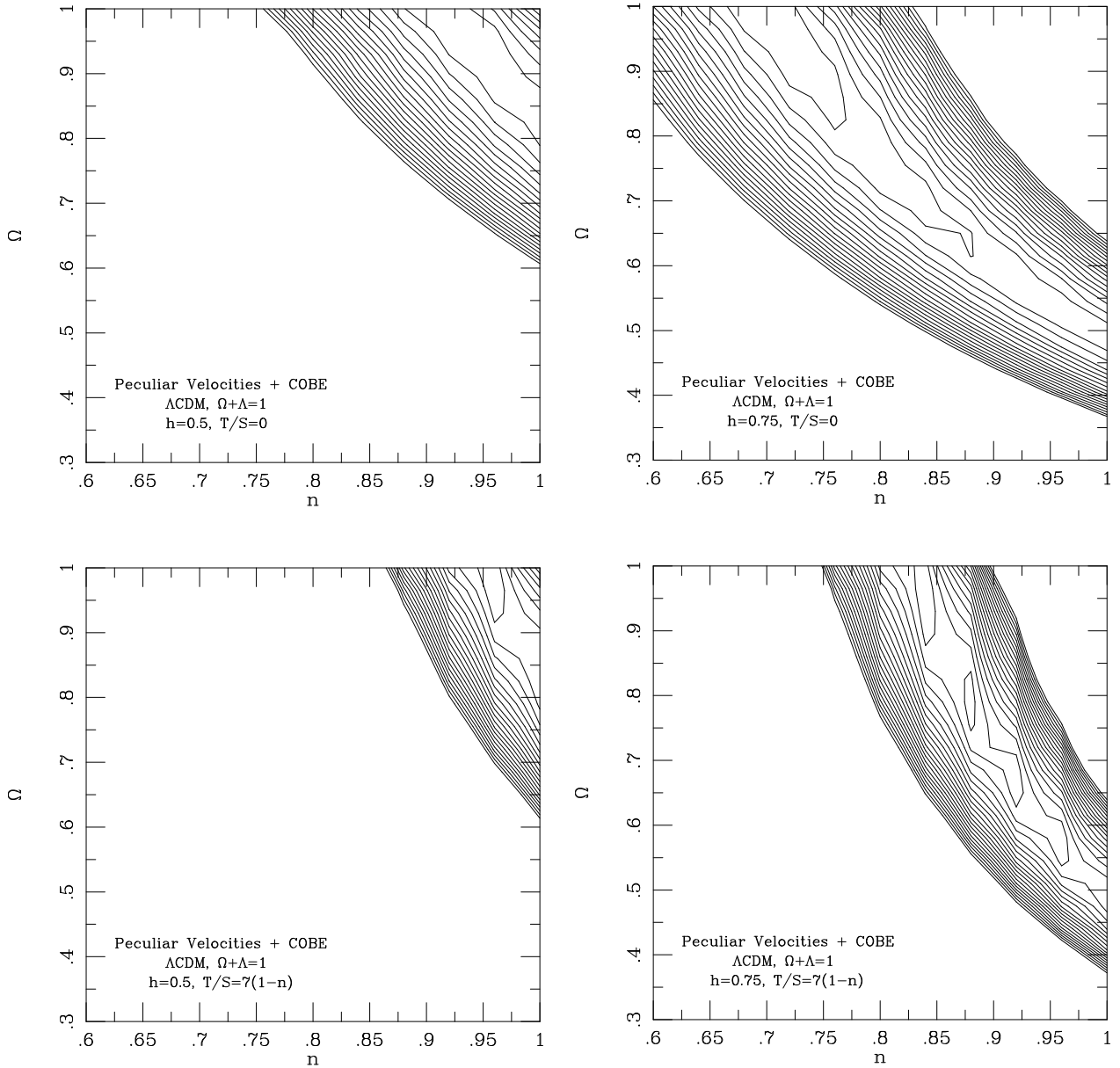


Figure 4: Contours of ln-likelihood in the $n - \Omega$ plane, calculated with $h=0.5$ and 0.75 for tilted- Λ CDM models, with and without tensor component. $\Delta[\ln \mathcal{L}] = -1$.

4.2.2 Tilted Models

Figure 4 shows the likelihood in the $n - \Omega$ plane for the tilted- Λ CDM family of models. The computation is done for fixed values of h at $h = 0.5$ or 0.75 , with or without tensor fluctuations. COBE normalization is by White and Bunn (1995). The elongated ridge of high likelihood can now be described by

$$\Omega h_{50}^{1.3} n^{2.0} = 0.83 \pm 0.12, \quad T/S = 0, \quad (13a)$$

$$\Omega h_{50}^{1.3} n^{3.4} = 0.83 \pm 0.12, \quad T/S = 7(1 - n). \quad (13b)$$

The trends along the ridges are, again, not robust to changing the data from G to S.

For a fixed Ω , this relation can be understood qualitatively as follows: the normalization by COBE fixes the amplitude at small wavenumbers, $k \sim 0.001$, and the velocity data constrain the amplitude at $k \sim 0.1$. The wavenumber corresponding to the peak of the PS is roughly proportional to Ωh . Therefore, if a good fit is obtained with certain values of h and n , a similarly good fit can be obtained with higher h and lower n , or vice versa. The presence of tensor fluctuations lowers the amplitude imposed by COBE at small wavenumbers, and thus weakens the requirement for a tilt in n .

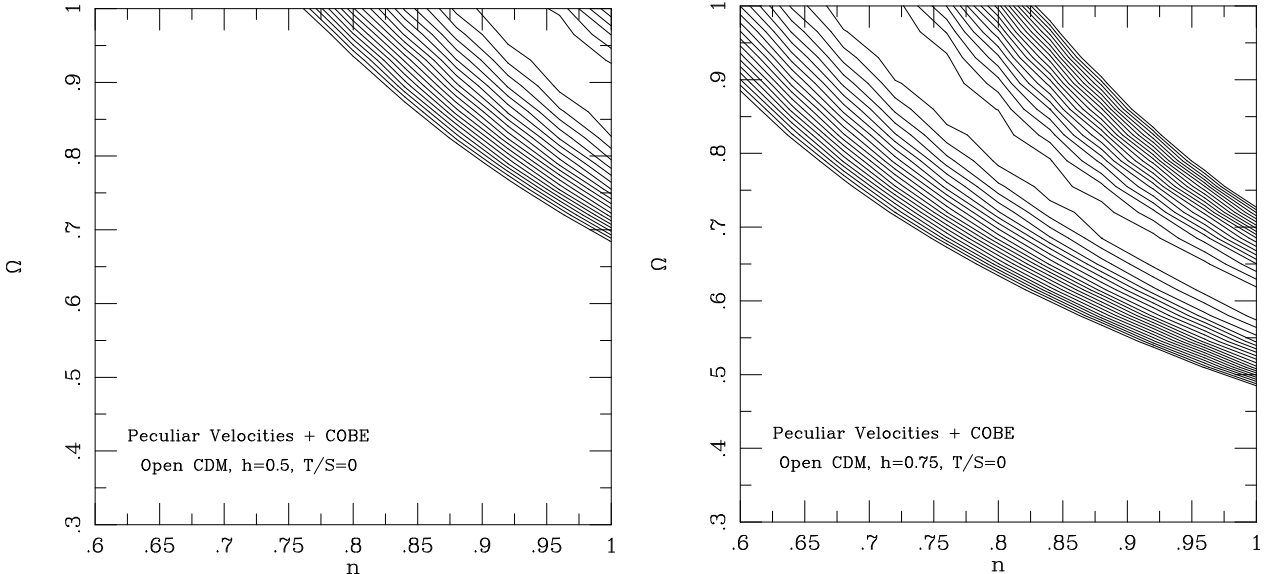


Figure 5: The same as Figure 4 for tilted Open CDM models without tensor component, $\Delta[\ln \mathcal{L}] = -1$.

Figure 5 shows the analogous likelihood results in the $n - \Omega$ plane for the tilted- Λ CDM family of models (normalized by Sugiyama 1995). Computations were done for the two values of h as before, but this time only for the case of no tensor fluctuations. The results are qualitatively similar to the case of tilted- Λ CDM models. The tight constraint for tilted- Λ CDM is

$$\Omega h_{50}^{0.95} n^{1.4} = 0.88 \pm 0.09. \quad (14)$$

In this case, the trends along the ridge of high likelihood are weak.

4.2.3 Model Dependence

The most likely PS for the tilted- Λ CDM family of models with tensor fluctuations and $h = 0.75$, corresponding to $\Omega = 0.97$ and $n = 0.84$, is plotted in Figure 6. The figure also shows the typical scatter in the PS about the most likely model, using $n - \Omega$ pairs that lie on the innermost likelihood contour (Fig. 4, lower-right panel). This scatter is somewhat smaller than in the Γ model (Fig. 2b), partly due to the additional constraint from COBE. Within this family of models, the constraints obtained are $P(k)\Omega^{1.2} = (4.2 \pm 0.8) \times 10^3 (h^{-1}\text{Mpc})^3$ at $k = 0.1 h \text{ Mpc}^{-1}$ and $\sigma_8 \Omega^{0.6} = 0.88 \pm 0.10$, where the error-bars are the likelihood analysis 90% confidence limits. The scatter in these quantities for the other CDM families of models is roughly the same.

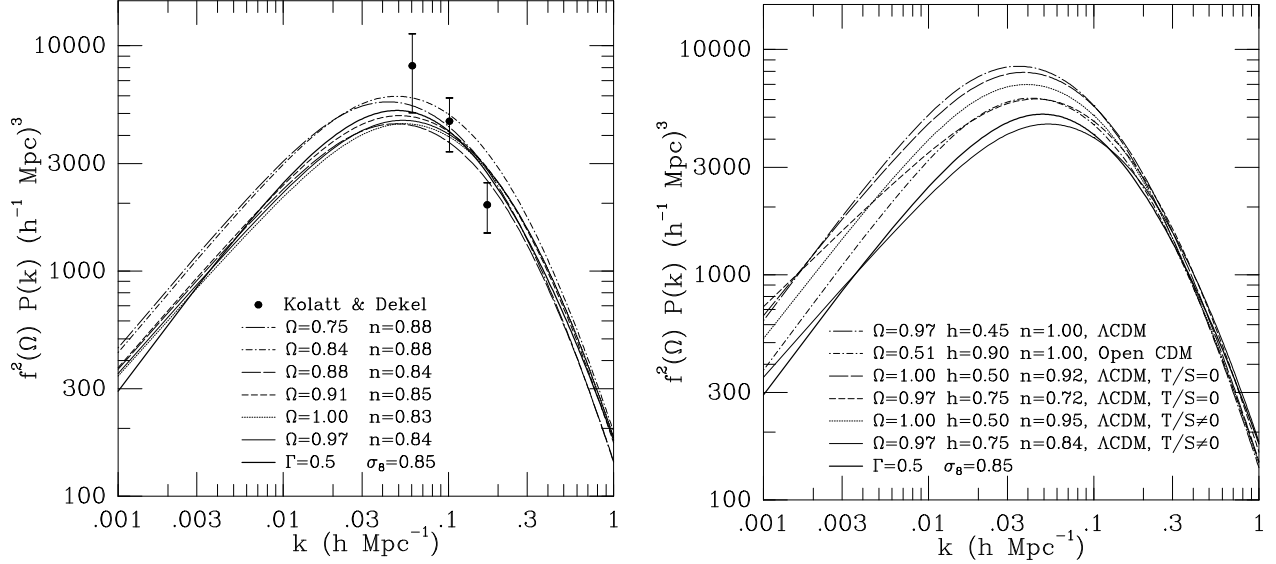


Figure 6: The PS of the most probable COBE-normalized CDM model (solid), and the scatter about it following parameter pairs that lie on the innermost likelihood contour (Fig. 4, lower-right panel). The COBE-free Γ model is also marked (heavy solid). The PS computed by KD from POTENT density of the same velocity data (independent of COBE or models), and their 1σ measurement errors, are shown in three bins.

Figure 7: The best-fit power spectra for various CDM models.

How robust are the results to the choice of model within the CDM families? Table 1 in Appendix A shows the features of the most likely models for each family of CDM variant discussed above, for the G catalog. Listed for each model is the corresponding value of $\sigma_8\Omega^{0.6}$, the amplitude of the PS at $k = 0.1 h \text{ Mpc}^{-1}$, the location of the peak and, most important, the functional fit to the high-likelihood ridge, in which the most likely model resides.

These power spectra of the best-fit models are plotted in Figure 7. All the models agree to within $\sim 20\%$ for $k > 0.1 h \text{ Mpc}^{-1}$, and they differ by up to $30 - 50\%$ on larger scales. The amplitude of the PS at $k = 0.1 h \text{ Mpc}^{-1}$ across the models is constrained to be $P(k)\Omega^{1.2} = (4.8 \pm 0.8) \times 10^3 (h^{-1}\text{Mpc})^3$. The value of $\sigma_8\Omega^{0.6}$ is roughly the same for all these models and ranges between 0.87 and 0.94.

Table 1 shows as well the $\ln \mathcal{L}$ value of each of these models (with the zero set arbitrarily to the highest likelihood). The best-fit models are all of comparable likelihood. The most likely model, with a small margin, is the tilted- Λ CDM model with tensor fluctuations and $h = 0.75$: $\Omega = 0.97$ and $n = 0.84$, the model plotted in Figure 6. This conclusion, however, is limited to the G catalog. For the S catalog, the preferred models are non-tilted ($n = 1$), with lower Ω ($\sim 0.6 - 0.7$) and h (~ 0.6) (see Table 2).

Figure 6 also compares the PS corresponding to the most-likely COBE-normalized CDM model and the most likely Γ model that is independent of COBE. The agreement between the two is within $\sim 10\%$ on all scales. The agreement on the location of the peak in the PS reflects the fact that the peculiar velocity data themselves contain some meaningful information on scales as large as the size of the Mark III sample even without the constraint from COBE.

The PS computed by KD from the POTENT smoothed density field, that has been recovered from the same Mark III data independent of COBE or models, is also displayed in Figure 6. The results (for all the models tested here) agree within 1σ of the measurement errors, and they agree particularly well near $k = 0.1 h \text{ Mpc}^{-1}$, where the velocity data imposes the strongest constraints. The spectral slope m near $k = 0.1 h \text{ Mpc}^{-1}$, as constrained by our method, is roughly $m = -0.75 \pm 0.45$. The KD spectrum appears to be steeper ($m \sim -1.5$), and the associated estimate of $\sigma_8 \Omega^{0.6}$ by KD is therefore marginally lower, at $\simeq 0.7 - 0.8$. In fact the KD slope is steeper than any of the CDM spectra discussed here (see Figure 7), and is roughly as steep as the PS predicted by the CHDM model, a 7:3 mixture of cold and hot dark matter (KD). This may indicate that the CDM family, with the exception of CHDM, does not allow enough freedom for a perfect fit on small scales. Also, our present results may be less reliable on small scales because, other than grouping, we do not make here any correction for nonlinear effects. On the other hand, the result of the current paper is probably more reliable than KD on large scales, because the likelihood method uses all the velocity data including the large-scale flows, while the POTENT density field is insensitive to the bulk velocity.

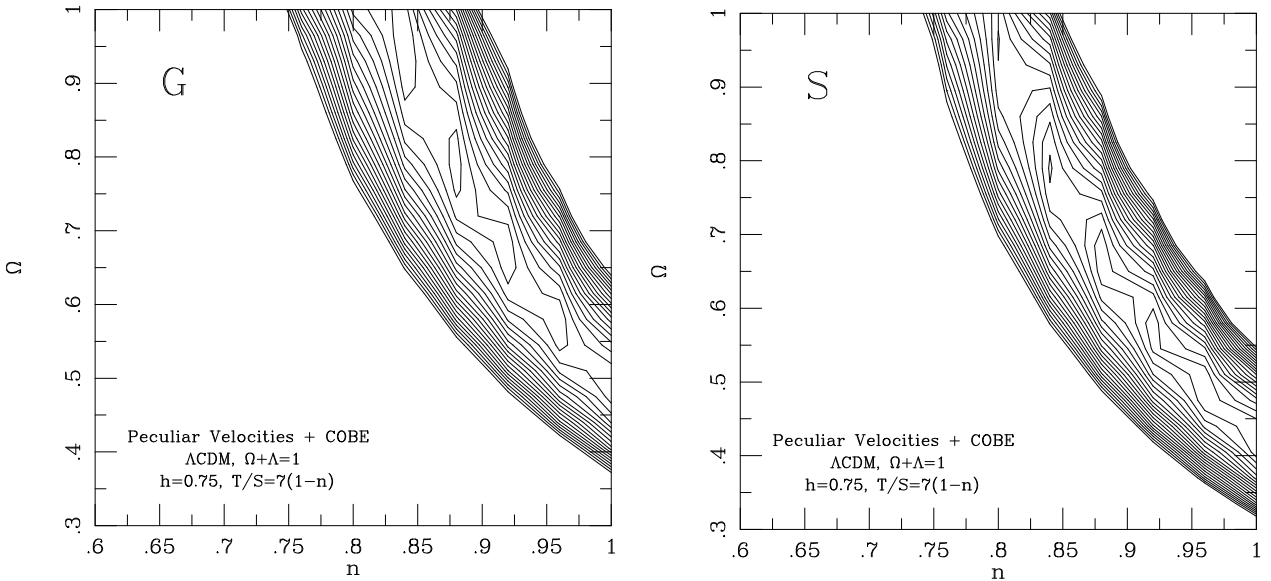


Figure 8: Contours of ln-likelihood in the $n - \Omega$ plane, calculated for tilted- Λ CDM model with a tensor component and $h=0.75$, obtained from the grouped data (G, same as Fig. 4, lower-right panel) and from the singles data (S). $\Delta[\ln \mathcal{L}] = -1$.

4.3. Robustness to Grouping in the Data

To test robustness to the grouping and Malmquist correction in the Mark III data, we have performed a similar likelihood analysis to the S catalog. Table 2 in Appendix A is the equivalent of Table 1 and summarizes the results for the S catalog. The S likelihood analysis might be more susceptible to small-scale non-linear effects that are not properly dealt with in our method. Still, it is interesting to compare the results for the G and S catalogs in order to distinguish further between robust and non-robust conclusions.

Figure 8 shows, as an example, the results obtained from the G and S catalogs for the tilted- Λ CDM model with tensor fluctuations and $h = 0.75$. The resemblance between these results is typical of the other models as well. First, the high-likelihood ridges are similar in shape: the powers μ and ν are almost the same in the G and S cases for all the CDM models we checked. Second, there is a slight difference in the constant defining the ridge: for the model plotted here the S result is $\Omega h_{50}^{1.25} n^{3.4} = 0.71 \pm 0.12$ while the G ridge was $\Omega h_{50}^{1.3} n^{3.4} = 0.85 \pm 0.12$, preferring somewhat higher values for the parameters. A similar trend occurs for all the models (see Appendix A).

The gradient of likelihood along the ridge is different for the G and S catalogs to the extent that it is sometimes of opposite sign. The G data slightly prefers a tilt in the spectrum and $\Omega \simeq 1$, while the S data slightly favors lowering the value of Ω below unity and $n \simeq 1$. This difference indicates that we should not assign high significance to the trends along the ridges of high likelihood and rather focus on the robust ridges themselves. We thus quote constraints on the degenerate combinations of Ω , h and n , and not on any of them separately.

The likelihood analysis of the S data with the Γ model also yields some differences. The maximum likelihood value is $\Gamma = 0.3 \pm 0.1$ for the S catalog, compared to the $\Gamma = 0.5 \pm 0.15$ for the G catalog. The shape parameter Γ (independent of COBE normalization) seems to be only poorly constrained by the data. Still, we can quote based on the velocity data alone that $\Gamma \geq 0.2$ at the 90% confidence level.

The robust feature for the Γ model is the value of $\sigma_8 \Omega^{0.6}$, which is stable at $\sigma_8 \Omega^{0.6} = 0.85 \pm 0.1$ for both the G and S catalogs. The lower Γ from the S data is accompanied by a higher amplitude A , such that the combination $\sigma_8 \Omega^{0.6}$ remains unchanged.

Another robust feature, for all models, is the amplitude of the maximum-likelihood power spectrum on intermediate scales. The PS amplitude at $k = 0.1 h \text{ Mpc}^{-1}$ for both S and G is constrained to be $P(k) \Omega^{1.2} = (4.8 \pm 1.5) \times 10^3 (h^{-1} \text{Mpc})^3$. The location of the peak in the PS in the two cases is roughly the same, ranging between 0.025 and $0.04 h \text{ Mpc}^{-1}$ for the S catalog, and between 0.03 and $0.06 h \text{ Mpc}^{-1}$ for the G catalog.

5. CONCLUSION

We have presented a Bayesian method for deriving the power spectrum of mass density fluctuations from the Mark III Catalog of Peculiar Velocities. The result is free of galaxy “biasing.” The method extracts the maximum amount of useful information from the data. It is exact to first order, under the assumption of Gaussian fluctuations and Gaussian errors. Tests using realistic mock catalogs show that this approximation is adequate because of the large-scale coherence of the velocity field and because the large errors that dominate on small scales make the nonlinear effects contribute only weakly to the result. The formal likelihood errors include both measurement errors and cosmic scatter. Ignored are the errors in the COBE normalization, of order of a few percent.

Our robust result for the whole family of models examined here as priors and for the different ways of handling the grouping of the data is that the mass PS amplitude at $k = 0.1 h \text{ Mpc}^{-1}$ is $P(k) \Omega^{1.2} = (4.8 \pm 1.5) \times 10^3 (h^{-1} \text{Mpc})^3$. The robust integral constraint

for the CDM family of models $\sigma_8\Omega^{0.6} = 0.88 \pm 0.15$. The errors quoted are crude: they reflect the typical 90% uncertainty for each of the best-fits within each family of models, combined with the typical scatter among these best-fit models and between the G and S treatments of the data. Similar results are obtained when using the velocity data alone and when the additional constraints from COBE are included. For the span of models checked, the PS peak is in the range $0.02 \leq k \leq 0.06 h \text{ Mpc}^{-1}$.

This normalization of the PS is in pleasant agreement with the independent ‘frequentist’ computation of the PS via POTENT by KD, which yielded $P(k)\Omega^{1.2} = (4.6 \pm 1.4) \times 10^3 (h^{-1} \text{Mpc})^3$ at $k = 0.1 h \text{ Mpc}^{-1}$, and $\sigma_8\Omega^{0.6} \approx 0.7 - 0.8$. Our new results differ at about the 2σ level from the earlier estimate by Seljak & Bertschinger (1994) of $\sigma_8\Omega^{0.6} = 1.3 \pm 0.3$. They performed a likelihood analysis of the POTENT reconstructed density field based on the earlier Mark II sample. The main improvements since then are that the current analysis includes five times denser sampling in a more extended volume, the systematic errors such as Malmquist bias are handled better, and a wider span of models and parameters is used in the likelihood analysis. It may be interesting to note that the current measurement is somewhat higher than the completely independent estimate of a similar quantity based on cluster abundances, $\sigma_8\Omega^{0.56} \simeq 0.57 \pm 0.05$ (White, Efstathiou, & Frenk 1993), but it is only about 2σ away.

The comparisons of the mass σ_8 to the values observed for optical galaxies ($\simeq 0.95$) and for IRAS 1.2Jy galaxies ($\simeq 0.6 - 0.7$) indicate β values of order unity to within 25% for most galaxy types on these scales (see KD, Fig. 6 and Table 2, for more details).

A Γ -shape model, free of COBE normalization, is constrained by the velocity data only weakly, to Γ in the range $0.2 - 0.6$. The most likely value of Γ are somewhat higher than the canonical values of $\sim 0.2 - 0.3$ typically obtained from galaxy density surveys (*e.g.* Efstathiou *et al.* 1992, Peacock & Dodds 1994).

Within the families of COBE-normalized CDM models, which we have restricted to the range $\Omega \leq 1$ and $n \leq 1$, we have obtained constraints on combinations of the cosmological parameters of the sort $\Omega h_{50}^\mu n^\nu = 0.8 \pm 0.2$, with $\mu = 1.3$ for the flat models and with $\nu = 3.4$ and 2.0 with and without tensor fluctuations respectively. For the open models without tensor fluctuations the corresponding powers are $\mu = 0.95$ and $\nu = 1.4$. The extended error quoted include the uncertainty due to measurement errors and finite sampling, the variation among the various CDM models, and the uncertainty in the best way to group the data for Malmquist correction.

The most likely model for the G data is a tilted- Λ CDM model with tensor fluctuations, relatively high Hubble constant ($h \sim 0.75$), Ω near unity and $n \sim 0.85$. These results are consistent with the conclusion of White *et al.* (1995), who argue for tilted CDM based on several data sets including power spectra of galaxy density (Peacock & Dodds 1994), cluster correlations, pair-wise velocities and COBE’s results. Their best fit is $\Omega = 1$, $h \approx 0.45$, $n = 0.9$, with tensor fluctuations. This model is about 1σ away from our best fit but the PS is quite similar. Our lower value of n compensates for the higher value of h .

It is interesting to note that based on the velocity data and COBE normalization alone, the standard CDM model ($\Omega = 1$, $n = 1$, $h = 0.5$) is less likely than its various

variants studied here (see Appendix A). A slight tilt in n or a small decrease of Ω can increase the likelihood significantly. However, this does not imply that the standard CDM model is necessarily ruled out as our analysis measures only relative likelihoods rather than absolute goodness of fit.

In a subsequent paper (Zaroubi *et al.* 1996), our range of allowed power spectra from the peculiar velocities is translated to an angular power spectrum of CMB fluctuations and compared to recent subdegree observations. We find there that in order to also fit the height of the first CMB peak with a CDM spectrum, the tilt cannot be more pronounced than $n \sim 0.9$, the total energy density $\Omega + \Lambda$ should be close to unity, and the baryonic fraction should be large, $\Omega_b \sim 0.1$. A discussion of our results in the wider context of cosmological parameters can be found in Dekel, Burstein & White (1997) and Dekel (1997).

It is worth recalling that the recovered power spectrum is highly sensitive to the assumed observational errors, because the noise has a systematic effect on the measured power spectrum. Effectively, the power spectrum of the errors has to be subtracted out. This can be done explicitly, as in KD, or implicitly, as in our current likelihood analysis. Our input error estimate is based on the careful error analysis of the Mark III data by Willick *et al.* (WI; WII; WIII). If, for some reason, this is an underestimate of the errors, then the recovered power spectrum is an overestimate, and vice versa.

Finally, a note of caution of technical nature about the method and its application to the current data under certain extreme conditions. If not enough constraints are imposed, the inversion of $\tilde{U}_{i,j}$ (Eq. 5) may become dominated by the noise rather than the signal and might lead to a wrong answer. We encountered this problem when we tried to parameterize the PS with a multi-parameter function that did not enforce any upper bound on the power on large scales (bounds that are properly enforced when COBE constraints are used, for example). The likelihood analysis preferred in this case unphysically high power on large scales. This is probably, at least in part, a result of noise dominance, and is beyond the scope of this paper. An algorithm to detect and possibly eliminate this problem is discussed elsewhere (Zaroubi 1995). As long as we use models that are properly bound on large scales the results on small scales are robust. The Γ model, for example, does not suffer from this problem because its shape effectively enforces the appropriate bounds on large scales. The data strongly constrain the amplitude $P_{0.1}$ and the slope near $k = 0.1 h \text{ Mpc}^{-1}$. A Γ model with the peak at a very small k and the same $P_{0.1}$ would have required a steeper slope ($m = -2$ to -3) which is disfavored by the data. The Γ model thus enforces specific connections between properties that are strongly constrained by the data with properties that are poorly constrained.

Acknowledgments

We thank Naoshi Sugiyama for providing the COBE normalizations for the CDM models prior to publication and for close interaction. We acknowledge stimulating discussions with Marc Davis, Ravi Sheth, Douglas Scott and Martin White. We thank the referee Robert Crittenden for helpful comments. YH and IZ acknowledge the hospitality of the Astronomy Department and the Center for Particle Astrophysics at Berkeley where part of this work was done. This work is supported in part by the US-Israel Binational

Science Foundation grants 92-00355, 95-00330 and 94-00185, by the Israel Science Foundation grants 469/92, 950/95 and 590/94, and by the US National Science Foundation grant PHY-91-06678. IZ has been partly supported by the Exchange of Astronomers Programme of the IAU.

APPENDIX A

We present here the detailed likelihood analysis results for the various COBE normalized CDM families of models. Table 1 shows the results obtained for the G catalog. The functional fit of the high-likelihood ridge obtained in each case is given. The error-bar quoted is the formal 90% confidence limit of the degenerate parameter combination. The values of the cosmological parameters corresponding to the maximum-likelihood model within this ridge are listed as well. Parameters that were held fixed in the likelihood analysis while varying the other parameters are denoted by “fixed”. For reference, the COBE normalized standard CDM model is also listed. The value of $\ln \mathcal{L}$ obtained for each of these models is given, with the zero set arbitrarily to correspond to the most likely model.

TABLE 1
Maximum-Likelihood Results of the G Catalog for CDM Models

CDM Model	Ridge	$\sigma_8 \Omega^{0.6}$	$P_{0.1} \Omega^{1.2}$	k_{peak}				
		(± 0.10)	(± 1000)	(± 0.015)	Ω	h	n	$\ln \mathcal{L}$
Standard		1.2	7700	0.042	1(fixed)	0.5(fixed)	1(fixed)	-8.80
Λ , $n=1$	$\Omega h_{50}^{1.3} = 0.83 \pm 0.09$	0.92	5600	0.035	0.97	0.45	1(fixed)	-2.34
Open, $n=1$	$\Omega h_{50}^{0.95} = 0.88 \pm 0.07$	0.87	4600	0.042	0.51	0.90	1(fixed)	-0.45
Tilted- Λ (T/S=0)	$\Omega h_{50}^{1.3} n^{2.1} = 0.83 \pm 0.12$	0.94	5600	0.037	1.00	0.5(fixed)	0.92	-1.97
	$\Omega h_{50}^{1.3} n^{1.9} = 0.83 \pm 0.12$	0.92	4800	0.044	0.97	0.75(fixed)	0.72	-0.78
Tilted- Λ (T/S \neq 0)	$\Omega h_{50}^{1.3} n^{3.6} = 0.83 \pm 0.11$	0.90	5100	0.039	1.00	0.5(fixed)	0.95	-1.19
	$\Omega h_{50}^{1.3} n^{3.4} = 0.85 \pm 0.11$	0.88	4100	0.053	0.97	0.75(fixed)	0.84	0.00
Tilted-Open (T/S=0)	$\Omega h_{50}^{0.95} n^{1.4} = 0.88 \pm 0.09$	0.91	5300	0.037	1.00	0.5(fixed)	0.92	-1.76
	$\Omega h_{50}^{0.95} n^{1.4} = 0.88 \pm 0.09$	0.91	4700	0.044	0.97	0.75(fixed)	0.72	-0.70

Several features of the power spectra of these best-fitting models are presented: the value of $\sigma_8 \Omega^{0.6}$, the amplitude of the PS at $k = 0.1 h \text{ Mpc}^{-1}$, $P_{0.1} \Omega^{1.2}$, and the location of the peak in the PS, k_{peak} . The quoted error-bars in the table headings represent the typical 90% likelihood uncertainty in these quantities within each family of models. Due to the high-likelihood ridge in each family of models, the exact location of the maximum-likelihood model within the ridge is hardly significant, but the table demonstrates the robust features among these models (see discussion in §4.2.3).

Table 2 lists the results of the various CDM models for the S catalog. Similar high-likelihood ridges are listed, though there is a small systematic shift toward smaller values in the constant defining the ridge compared to the G data. The trends along the ridges and the likelihood ranking of the various models are different then in the G case but, again, they are only marginally significant. However the general features of the PS, such as the values of $\sigma_8\Omega^{0.6}$ and $P_{0.1}\Omega^{1.2}$, are similar (see §4.3).

TABLE 2
Maximum-Likelihood Results of the S Catalog for CDM Models

CDM Model	Ridge	$\sigma_8\Omega^{0.6}$	$P_{0.1}\Omega^{1.2}$	k_{peak}	Ω	h	n	$ln\mathcal{L}$
		(± 0.10)	(± 1000)	(± 0.015)				
Standard		1.2	7700	0.042	1(fixed)	0.5(fixed)	1(fixed)	-40
Λ , $n=1$	$\Omega h_{50}^{1.25} = 0.69 \pm 0.07$	0.86	5300	0.030	0.55	0.60	1(fixed)	-0.01
Open, $n=1$	$\Omega h_{50}^{0.9} = 0.78 \pm 0.06$	0.83	4800	0.033	0.90	0.42	1(fixed)	-0.24
Tilted- Λ ($T/S=0$)	$\Omega h_{50}^{1.25} n^{1.9} = 0.69 \pm 0.09$	0.86	5300	0.031	0.69	0.5(fixed)	1.00	0.00
	$\Omega h_{50}^{1.25} n^{1.9} = 0.70 \pm 0.09$	0.86	5200	0.033	0.55	0.75(fixed)	0.88	-0.20
Tilted- Λ ($T/S \neq 0$)	$\Omega h_{50}^{1.25} n^{3.4} = 0.69 \pm 0.12$	0.84	5200	0.031	0.69	0.5(fixed)	1.00	-0.02
	$\Omega h_{50}^{1.25} n^{3.4} = 0.71 \pm 0.12$	0.83	4800	0.032	0.48	0.75(fixed)	0.96	-0.39
Tilted-Open ($T/S=0$)	$\Omega h_{50}^{0.9} n^{1.5} = 0.76 \pm 0.08$	0.84	4800	0.034	0.76	0.5(fixed)	1.00	-0.28
	$\Omega h_{50}^{0.9} n^{1.3} = 0.80 \pm 0.08$	0.83	4500	0.039	0.55	0.75(fixed)	1.00	-1.10

REFERENCES

- Bardeen, J. M., Bond, J. R., Kaiser, N., & Szalay, A. S. 1986, *Astrophys. J.*, 304, 15
 Bennett, C. L., *et al.* 1996, *Astrophys. J.*, 464, L1
 Bertschinger, E., & Dekel, A. 1989, *Astrophys. J.*, 336, L5
 Crittenden, R., Bond, J. R., Davis, R. L., Efstathiou G., & Steinhardt, P. J. 1993, *Phys. Rev. Lett.*, 61, 324
 Dekel, A. 1994, *Ann. Rev. of Astron. & Astrophys.*, 32, 371
 Dekel, A., 1997, in *Formation of Structure in the Universe*, ed. A. Dekel & J. P. Ostriker (Cambridge: Cambridge University Press), in press
 Dekel, A., Bertschinger, E., & Faber, S. M. 1990, *Astrophys. J.*, 364, 349
 Dekel, A., Burstein, D., & White, S. D. M. 1997, in *Critical Dialogues in Cosmology*, ed. N. Turok (Princeton: Princeton University Press), in press
 Dekel, A., & Rees, M. J. 1987, *Nature*, 326, 455

- Dressler, A. 1980, *Astrophys. J.*, 236, 351
- Efstathiou, G., Bond, J. R., & White, S. D. M. 1992, *M.N.R.A.S.*, 258, 1p
- Górski, K. M. 1988, *Astrophys. J.*, 332, L7
- Górski, K. M., Ratra, B., Sugiyama, N., & Banday, A. J. 1995, *Astrophys. J.*, 444, L65
- Jaffe, A. H., & Kaiser, N. 1995, *Astrophys. J.*, 455, 26
- Kaiser, N. 1987, *M.N.R.A.S.*, 227, 1
- Kaiser, N. 1988, *M.N.R.A.S.*, 231, 149
- Kolatt, T., & Dekel, A. 1996, *Astrophys. J.*, in press (astro-ph/9512132)
- Kolatt, T., Dekel, A., Ganon, G., & Willick, J. 1996, *Astrophys. J.*, 458, 419
- Peacock, J. A., & Dodds, S. J. 1994, *M.N.R.A.S.*, 267, 1020
- Press, W. H., Teukolsky, S. A., Vetterling, W. T., & Flannery, B. P. 1992, "Numerical Recipes" (2d ed.; Cambridge: Cambridge University Press)
- Seljak, U., & Bertschinger, E. 1994, *Astrophys. J.*, 427, 523
- Sugiyama, N. 1995, *Astrophys. J. (Supp.)*, 100, 281
- Turner, M. S. 1993, *Phys. Rev.*, D48, 5302
- Tytler, D., Fan, X-M., & Burles, S. 1994, *Nature*, 381, 207
- White, M., & Bunn, E. F. 1995, *Astrophys. J.*, 450, 477
- White, M., Scott, D., Silk, J., & Davis, M. 1995, *M.N.R.A.S.*, 276, 69P
- White, S. D. M., Efstathiou, G., & Frenk, C. S. 1993, *M.N.R.A.S.*, 262, 1023
- Willick, J. A., Courteau, S., Faber, S. M., Burstein, D., & Dekel, A. 1995, *Astrophys. J.*, 446, 12
- Willick, J. A., Courteau, S., Faber, S. M., Burstein D., Dekel, A., & Kolatt, T. 1996a, *Astrophys. J.*, 457, 460
- Willick, J. A., Courteau, S., Faber, S. M., Burstein, D., & Dekel, A. 1996b, *Astrophys. J. (Supp.)*, in preparation
- Zaroubi, S. 1995, in Proc. of the XXXth Rencontres de Moriond "Clustering in the Universe", ed. S. Maurogordato, C. Balkowski, C. Tao & J. Trần Thanh Vân (Gif-sur-Yvette Cedex: Editions Frontieres), 135
- Zaroubi, S., & Hoffman, Y. 1996, *Astrophys. J.*, 462, 25
- Zaroubi, S., Hoffman, Y., & Dekel, A. 1996, preprint
- Zaroubi, S., Hoffman, Y., Fisher, K. B., & Lahav, O. 1995, *Astrophys. J.*, 449, 446
- Zaroubi, S., Sugiyama, N., Silk, J., Hoffman, Y., & Dekel, A. 1996, *Astrophys. J.*, submitted (astro-ph/9610132)